Journal of Ceramic Processing Research. Vol. 18, No. 8, pp. 604~610 (2017)

J O U R N A L O F
Ceramic
Processing Research

The formation of magnetic properties in slag glass-ceramic and the effect on performance

Zhang Hongxia[a], Du Yongsheng[a,]*, Yang Xiaowei[a], Ouyang Shunli[b] and Li Baowei[b]
[a]*College of Science, Inner Mongolia University of Science &Technology, Baotou 014010, China*
[b]*Key Laboratory of Integrated Exploitation of Bayan Obo Multi-Metallic Resources, Inner Mongolia University of Science and Technology, Baotou 014010, China*

Ferrimagnetic glass-ceramics based on the CMAS system are successfully prepared by melting method, using two hazardous industrial wastes as starting materials. Influences of iron oxide additions on various properties in the slag glass-ceramics have been investigated by using DSC, XRD, STEM, HRTEM, SEM, RUS and VSM. The results indicate that the main crystalline phases of the glass-ceramics are augite and the initial nucleation phases are magnetite. Augite as a major crystalline phase and magnetite as a minor phase are precipitated with high iron oxide content. The comprehensive properties of glass-ceramics show a decreased tread with the gradual increase of the iron oxide content. The experimental data of magnetic hysteresis cycles at room temperature are analyzed with a maximum applied magnetic field of 20 kOe. It can be noted that the variations of hysteresis parameters in the glass-ceramics are largely dependent on content of magnetite phases.

Key words: Bayan Obo east mine tailing, Glass-ceramics, Augite, Magnetite, Magnetic properties.

Introduction

With the rapid development of the mining industry and the power industrial, the environmental damage caused by the accumulation and discharge of all kinds of solid waste has received extensive attention. At present, the method of treatment and comprehensive utilization of large amount of above-mentioned solid wastes include recycling and utilization of tailing, utilization as building materials, road construction or filling of metal mine goafs, which cannot realize cleaning, high value and efficient utilization of solid wastes. Among these different approaches, the possibility of high value-added treatment of solid wastes into glass-ceramics can be confirmed. This is because glass-ceramics present good mechanical properties, and it can be used as structure material in machinery, chemicals and other industries [1-3]. In our previous work [4-6], high corrosion resistance and wear resistance glass-ceramics are successfully obtained by melting method, using Bayan Obo mine tailing, blast furnace slag and fly ash as major raw material. The properties of slag glass-ceramics are as follows: the bending strength is 196 MPa, the Vickers hardness is 7.17 GPa, and the abrasion loss is reached 0.04 g/cm^2. The high-performance in glass-ceramics is attributed to multiple nucleating agents which intergrowth in Bayan Obo east mine [7-8].

It is generally known that the iron contribute to the formation of magnetite crystal in glass-ceramics which may serve as nuclei during the initial nucleation stage [9-11]. Karamanov et al. reported that Fe and Zn were concentrated in specific areas during the cooling of the melt and these areas became sites for the precipitation of magnetite and franklinite during the thermal treatment. In the surrounding zones, where the Si concentration was higher the formation of the pyroxene was favored [12]. Meanwhile, the magnetite phase and the main crystalline phase can exist simultaneously in glass-ceramics with high iron oxide content, and the reason for the magnetic properties of glass-ceramics can be explained as the appearance of magnetite [13-16]. The magnetic glass-ceramics with high mechanical characteristics are suitable for a wide range of applications and can be applied in absorbing materials, insulation materials and metal matrix composite materials. However, the lack of necessary experimental characterization on the formation of magnetite and the relationship between the magnetite and the main crystal phase in glass-ceramics is not conducive to people's understanding of the magnetic origin of glass-ceramics. In addition, the influences of magnetite phase on the properties of glass-ceramics have not been comprehensive investigated in previous studies. Thus, in this work, in order to investigate deeply the influence of magnetite on the crystallization characteristics, magnetic and mechanical properties of glass-ceramics, the tailing glass-ceramics with different ratio of iron

*Corresponding author:
Tel : +86-472-5954358
Fax: +86-472-5954358
E-mail: 46588582@qq.com

oxide are prepared and the nucleation and crystallization process of glass-ceramics, the formation of magnetite and its influence on elastic modulus, acid-resistance and bending strength are discussed in detail.

Experimental

Samples preparation

The experimental Bayan Obo east mine tailing and fly ash were obtained from Baotou Iron and Steel Company of China and Huadian Generating-Electricity Co., Ltd, respectively and the major chemical compositions were shown in our previous study [17]. The 42.3 wt% of tailing and 17 wt% of fly ash were used as raw materials to prepare CaO-MgO-Al_2O_3-SiO_2 (CMAS) glass-ceramics and the base glass composition was chosen as 42.60% SiO_2, 27.20% CaO, 3% MgO and 5.50% Al_2O_3 (weight ratio). Where, small amounts of SiO_2, Al_2O_3, MgO, and CaO (chemical grade) were added to make up the base glass composition. Five batches (sample nos. C-1, C-2, C-3, C-4, C-5) with different iron oxide additions were prepared and the total iron content in samples are about 9.2, 11.1, 13.1, 14.9, and 16.6 wt%, respectively.

The manufacturing process of glass-ceramics included glass melting, annealing, stage of nucleation and crystal growth. Firstly, Bayan Obo east mine tailing, fly ash and other additives after thorough mixing were melted in an electric furnace at 1450 ºC and held for 3 h at this temperature for homogenization in a corundum crucible. The melts then were cast into preheated stainless steel molds and subsequent annealing at 600 ºC for 2 h. Whereafter, nucleation and crystallization treatments were carried out in a muffle furnace for the annealed glass samples, and the nucleation and crystallization temperature (T_p) were determined by differential scanning calorimetry (DSC) measurement. Finally, the obtained glass-ceramics were cut into the desired dimension in order to perform different measurements.

Characterization

Thermo behaviors of the parent glasses directly cast in water were examined by a differential scanning calorimetry (DSC) measurement (NETZSCH DSC 404 F3), applying temperature accelerating rate of 10 ºC/min. The phase constituents of the glass–ceramics were identified by X-ray powder diffraction (XRD, Bruker diffractometer, AXS D8 ADVANCED). The microscopic structures were investigated by scanning electron microscope (SEM, Philips, Quanta 400). The fine structure of glass-ceramics was investigated using transmission electron microscope (TEM, Tecnai G2 F20 STwin) at 200 kV acceleration voltage. Energy dispersive X-ray (EDX) was employed to identify the chemical composition of the crystalline phases and glass phases. Scanning electron microscope (SEM, Hitachis-3400) was used to observe the microstructure and morphology of glass-ceramics, which had been polished and etched in 3% HF acid for 60 sec and then coating with gold. Elastic constants of the glass–ceramics, including elastic modulus(E), shear modulus(G) and Poisson's ratio(ν), were measured using resonant ultrasound spectroscopy (RUS). Bending strength of the glass-ceramics with dimensions of 3 mm × 4 mm × 40 mm was measured by applying three point bending method through the CSS-88000 electronic universal testing machine. Five samples were measured and the results are the mean value of these tests. The bulk densities were measured by the Archimedes method. The corrosion test was evaluated with the cast stone standard JC/T258-1993 in concentration of 20% H_2SO_4 within water bath heating of 100 ºC. The glass-ceramics samples were crushed and the diameter of glass-ceramic pellets is about 0.5 mm-1.0 mm. Room temperature magnetisation of the rectified parallelepiped bars (2 mm × 5 mm × 5 mm) of glass–ceramics were determined using a vibrating sample magnetometer (VSM, Lakeshore 7407) and the magnetic hysteresis loop of glass-ceramics were obtained using external magnetic fields of ± 20 kOe.

Results

DSC plot of parent glass

Fig. 1 shows the DSC plot of parent glass sample C-1. Apparent transition temperature (T_g) at 635 ºC is observed, followed by two crystallizing exothermic peak at 745 and 825 ºC, respectively. Thus, a conventional two stage-heat treatment can be performed and the nucleation and crystallization temperatures are selected as 720 ºC and 850 ºC, respectively. Both of the above duration of heat treatment is 2hrs.

Crystallization characteristics of glass-ceramics

Fig. 2 presents the XRD patterns of the samples with different iron oxide additions subjected to sequential heat treatments. Where the annealed sample without

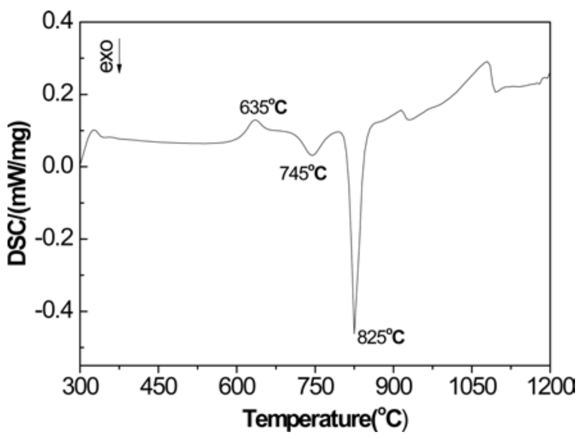

Fig. 1. DSC curves of the parent glass.

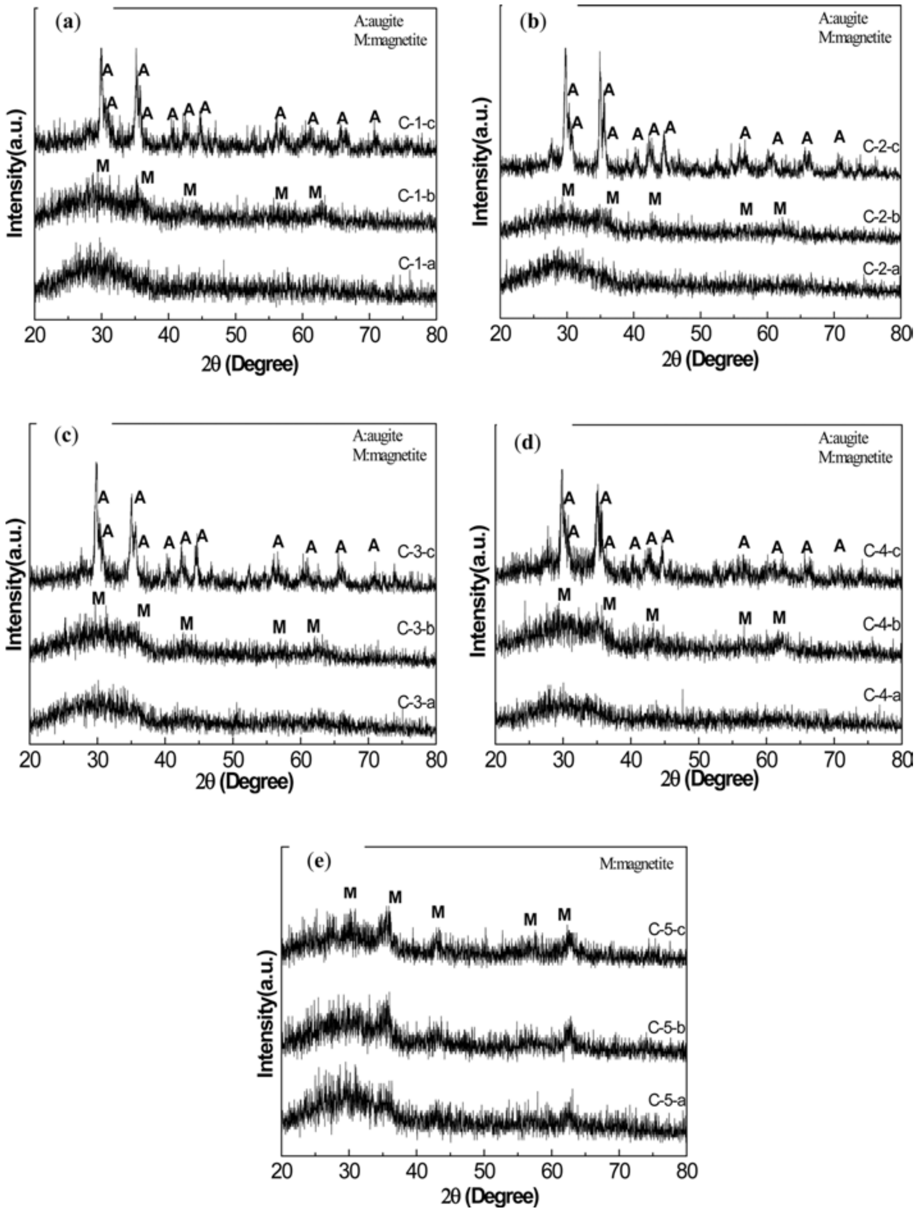

Fig. 2. XRD spectra of glass-ceramics with different nucleation process; (a) sample C-1, (b) sample C-2, (c) sample C-3, (d) sample C-4 and (e) sample C-5.

nucleation process is represented by the letter a, and Letters b and c represent the samples after nucleation treatment and the duration of the treatment is zero (heat the temperature to 720 ºC and put into water immediately) and 2 h, respectively. The samples of C-1-a, C-2-a, C-3-a and C-4-a has only glassy structure due to the appearance of a broad halo and the absence of any diffraction peaks associated with crystalline phases. The weak peaks of magnetite (Fe_3O_4, JCPDS 89-688) appear in the initial stages of nucleation process for samples C-1-b, C-2-b, C-3-b and C-4-b. After the nucleation treatment for 2 hrs, the samples' crystallinity change obviously and the intensity is relatively higher. It can be found that the peaks of augite ($Ca(Mg,Fe,Al)_2(Si,Al)_2O_6$, JCPDS 89-5691) appear in nucleation treatment for 2 hrs. In contrast to above samples, the magnetite has appeared in the annealed sample C-5-a. However, the crystalline phase of sample C-5-c is still magnetite compared with other samples nucleation treatment for 2 hrs.

In order to observe the precipitation of crystalline phases in the process of nucleation, scanning transmission electron microscope (STEM) of sample C-1-b is shown in Fig. 3. White droplets are distributed in the glass matrix uniformly and it can be regarded as Fe-rich phase since bright areas contain elements having a higher atomic number from STEM image [18]. Further, based on the results of XRD analysis, these white small droplets sized 5-10nm may be magnetite crystal nuclei.

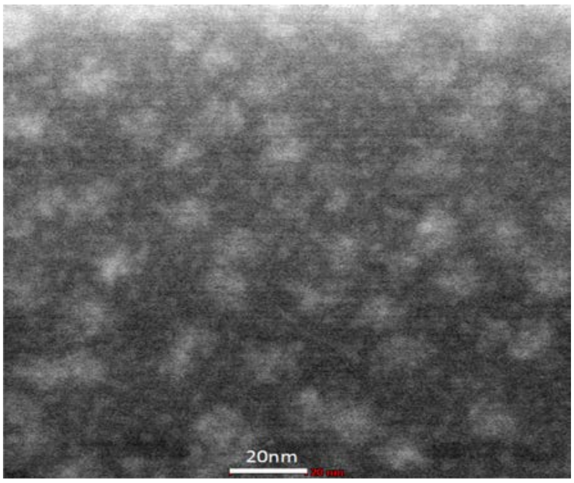

Fig. 3. STEM image of sample C-1-b.

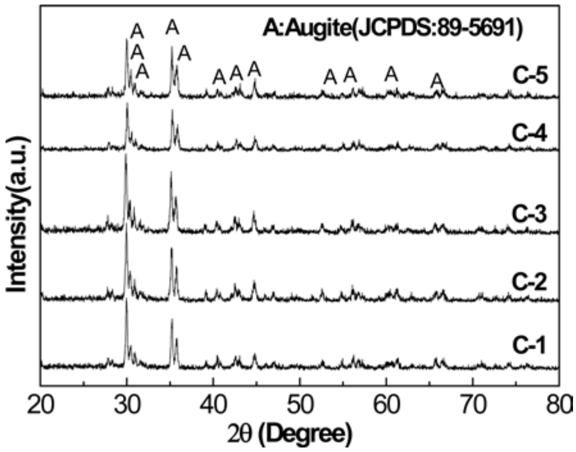

Fig. 4. XRD pattern of glass-ceramics after the crystallization treatment with different iron oxide additions.

Fig. 4 presents the XRD patterns of the glass samples subjected to crystallization treatment. It can be found that the main crystalline phase of the glass-ceramics is augite and the degree of crystallization of glass-ceramics with different iron oxide additions has no significant difference. In addition, the angle of

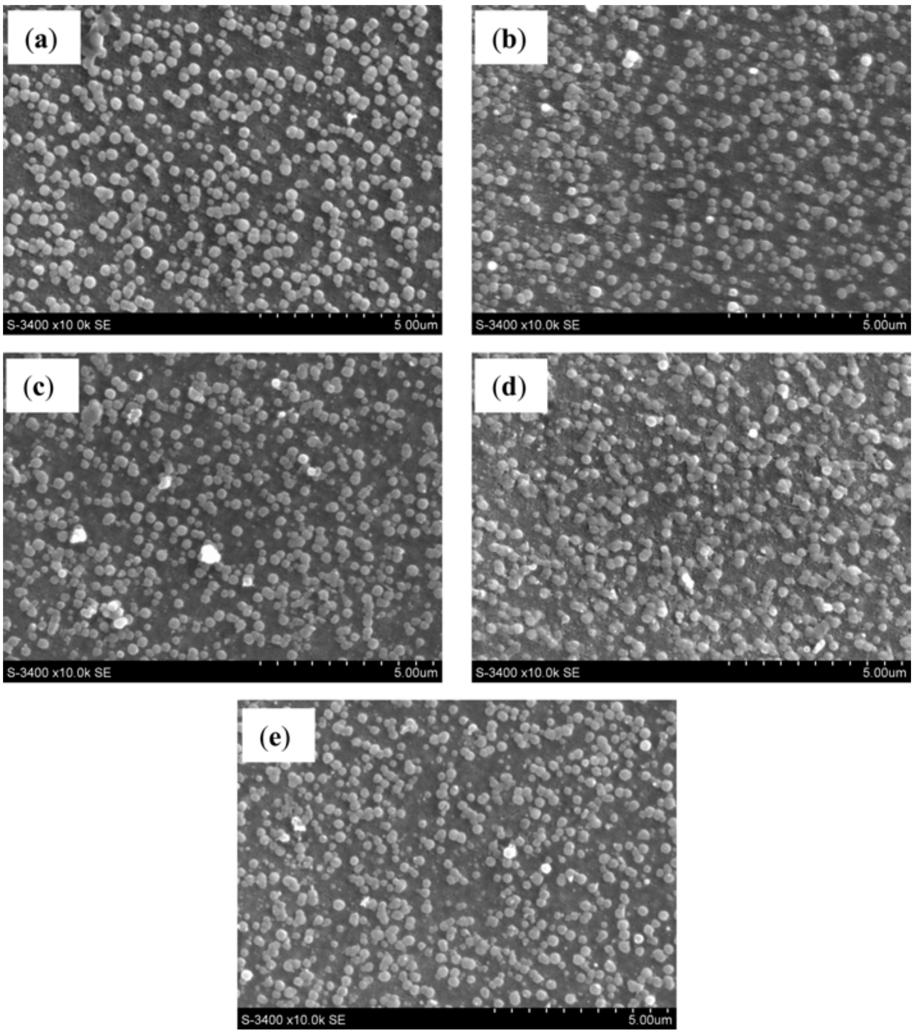

Fig. 5. SEM microstructures of glass-ceramics with different iron oxide additions after the crystallization treatment:(a) sample C-1, (b) sample C-2, (c) sample C-3, (d) sample C-4 and (e) sample C-5.

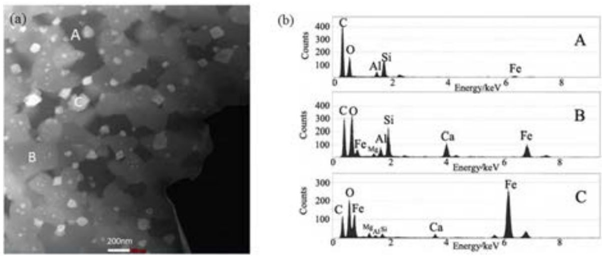

Fig. 6. (a) STEM image of sample C-5 and (b) corresponding EDX spectra of sample.

diffraction peaks in main crystal phase in samples C-4 and C-5 are displaced to right.

SEM images of the glass-ceramics with different amount of iron oxide addition after the crystallization treatment are shown in Fig. 5. It can be found that a large number of evenly distributed crystallites with a diameter of 200-300 nm are uniformly distributed in glass matrix. The shape and size of grain, the degree of crystallization of glass-ceramics have no great differences with different iron oxide additions. The results are in good agreement with the XRD results.

In order to characterize accurately the phase composition of the crystal, the STEM micrograph along with the EDX spectra of sample C-5 are shown in Fig. 6. It can be found that the composition of glass-ceramic consist of the main phase of augite, residual glass matrix and secondary phase of magnetite. That is, the magnetite phase and augite phase can exist simultaneously in glass-ceramics with high iron oxide content.

To investigate the microstructures of glass-ceramic specimens, high resolution transmission electron microscopy (HRTEM) images of C-5 specimen have been performed in Fig. 7. It clearly displays a well-defined lattice structure of the precipitated augite and magnetite and interplanar distances can be measured in HRTEM micrographs. The measured value of the lattice spacing for augite and magnetite is about 0.287 and 0.480 nm. the longest, measuring 0.480 nm corresponds to the (111) Bragg plane reflection of magnetite and the shortest one, measuring 0.287 nm is assigned to the ($\bar{3}11$) Bragg plane reflection of augite.

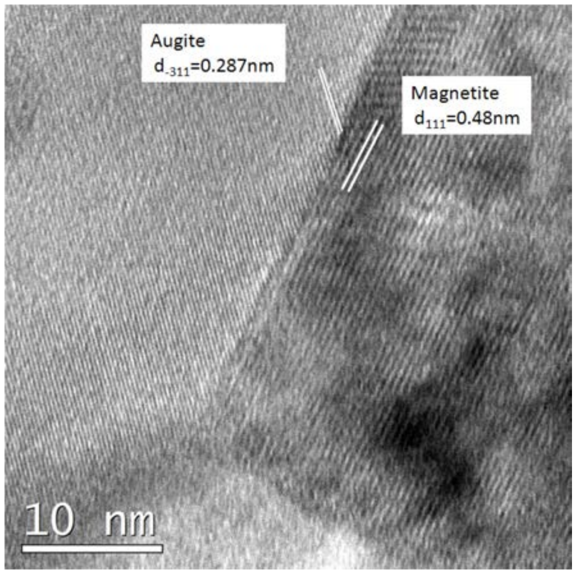

Fig. 7. HRTEM image of sample C-5.

Properties of the glass-ceramics with different iron oxide additions

In order to assess the impact of different iron oxide additions on properties of the glass-ceramics, the bending strength, acid-resistance and modulus of all samples are detected and analyzed. It can be found from Table 1 that the comprehensive properties of glass-ceramics show a decreased tread with the increase of iron oxide content. That is, the bending strengths, acid-resistance, elastic modulus and shear modulus all decrease with iron oxide increasing. Meanwhile, with the increase of iron oxide content, the density and Poisson's ratio in glass-ceramics show a trend to higher values.

Obvious magnetic hysteresis loops (M-H curves) are observed at different ratio of iron oxide as shown in Fig. 8 and the reported results are summarized in Table 2. It is generally known that concentration of magnetic phase has a direct effect on saturation magnetization (M_s). The remanence and coercivity represent ability of a ferromagnetic material which can be spontaneously magnetized and withstand an external magnetic field, respectively [19-20]. It can be seen that the saturation magnetisation (M_s), the coercivity force(H_{ci}) and remanent magnetization (M_r) tend to increase with the

Table 1. The properties of glass-ceramics with different iron oxide additions.

Sample no.	Bending strengths (MPa)	Density (g·cm^{-3})	Acid-resistance (%)	Elastic modulus (GPa)	Shear modulus (GPa)	Poisson's ratio
C-1	181.1	2.97	92.7	131.96	46.83	0.214
C-2	180.9	3.02	92.5	127.36	43.28	0.224
C-3	175.9	3.03	90.8	123.74	40.37	0.248
C-4	174.5	3.08	89.3	102.62	38.67	0.264
C-5	172.8	3.12	88.9	95.54	35.41	0.287

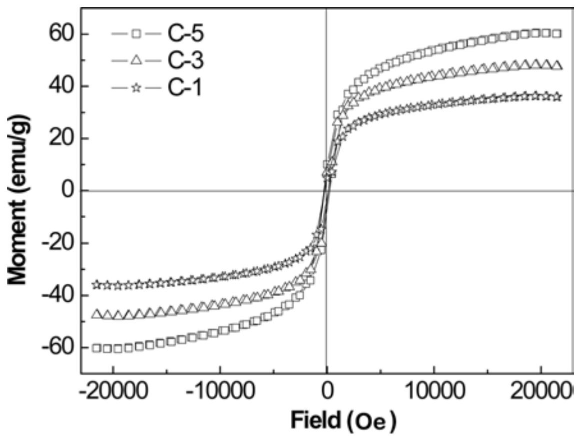

Fig. 8. M-H plot of the glass-ceramic bulk sample with different iron oxide additions.

Table 2. Magnetic parameters estimated from hysteresis cycles.

Sample no.	Saturation magnetization M_s (emu/g)	Coercive force H_{ci} (Oe)	Remanent magnetization M_r (emu/g)
C-1	36.3	169.4	4.8
C-3	47.8	178.1	6.8
C-5	60.4	269.2	9.6

gradual increase of the iron oxide content. So, the sample of C-5 has exhibited the highest magnetization. This can be attributed to the increase in the amount of magnetite with iron oxide [21].

Discussion

Crystallization characteristics

It can be deduced from DSC curves that the small exothermic peak is associated with the temperature that generate large amounts of crystal nucleus throughout the inside of the glass and the large exothermic peak (T_p) is associated with the production of crystal growth at a reasonable growth rate [22]. The two exothermic crystallization peaks could be associated to the formation of magnetite nuclei and augite combined with the results of XRD and STEM. Thus, the magnetite can act as the core of nucleation, and it provides growing conditions for main crystal phases of augite to deposit and grow. It can be found that the main crystalline phases of the glass-ceramics are all augite after the crystallization treatment and the addition of iron oxide does not change the main crystal phase from the results of XRD and SEM. In our experiment, iron oxide intergrowth in Bayan Obo east mine can provide plentiful nucleation centers of the glass during heat treatment [23]. With increase of the content of iron oxide, it can be found in our results that the diffraction peaks of the augite gradually shift to right and the possible explanation can be the increase of iron ions in augite structure. Since the augite usually contains calcium ions, magnesium ion and iron ion and so on, the cations of Ca^{2+} and Mg^{2+} are substituted for Fe^{3+} and Fe^{2+} in their normal sites with the increase of iron oxide. A decrease in the lattice parameter of augite can be found due to a relatively small radius of iron ions and the diffraction peaks shift to higher 2θ values.

The present investigation also reveal that, the addition of iron oxide is beneficial for the precipitation of magnetite and the formation of magnetite phase may be explained as the existence of amounts of iron oxide. The experimental results show that the appearance of main phase precipitation is delayed in sample C-5-c after the nucleation treatment, which indicate that the content of magnetite crystal nucleus increase. STEM micrograph and EDX analysis of sample C-5 indicate the magnetite phase and the main crystalline phase can exist simultaneously in glass-ceramics with high iron oxide content.

Mechanical and magnetic properties

The mechanical properties and magnetic properties of glass-ceramics samples are listed in Table I and II. In general, the elastic modulus, shear modulus and Poisson's ratio are considered to be important for the characterization of elastic properties of materials [24]. It is well known that the Poisson's ratios of oxide crystalline materials are usually 0.2-0.3. The glasses can be divided into resilient glasses ($0.15 < \nu < 0.20$), semi-resilient glasses ($0.20 < \nu < 0.25$), easily damaged glasses ($0.25 < \nu < 0.33$) [25]. The shear modulus is one of several quantities for measuring the stiffness of materials and the elastic modulus is a number that measures an object's resistance to being deformed elastically. The data reveal that the addition of iron oxide has increased the magnetic properties, but decrease the mechanical properties. This could be explained due to the development of magnetite phase instead of augite phase in the samples. Generally, the mechanical properties are loosely related to phase composition and microstructure, which both depend on the composition of the glass-ceramics, along with the additional agents, such as nucleation agents [26-27]. Combined with XRD and VSM characterization, the addition of iron oxide is beneficial for the precipitation of magnetite. Glass-ceramics with augite as main crystalline phases attract interest in several advanced fields as they offer excellent mechanical properties [28]. The glass-ceramics with magnetite as the main crystalline phases have poor performance compared with the performance of glass-ceramics with augite as the main crystalline phases. By contrast, the magnetic properties of glass-ceramics depend on the concentration of magnetite phase. Thus, the increase in the ratio of augite/magnetite is helpful to the enhancement of the performance, while the decrease in the ratio of augite/magnetite is beneficial to the increase of magnetic properties.

Conclusions

The crystallization behavior and properties in CMAS glass-ceramics derived from Bayan Obo east mine tailing have been investigated as a function of different iron oxide additions. The XRD and DSC analysis, the STEM images confirm the generation of the magnetite crystal nuclei, and magnetite can provide plentiful nucleation center for the consequent precipitation of augite crystalline. With the increase of iron oxide content, the mechanical properties of glass-ceramics decrease and the magnetic properties increase gradually which can be explained by the increase of magnetite/ augite ratio.

Acknowledgments

Foundation Item: Item Sponsored by Natural Science Foundation of Inner Mongolia Autonomous Region(Grant no.2017MS0507), National Natural Science Foundation of China (Grant no.11564031), Major Project of Chinese National Programs for Fundamental Research and Development (973 Program, Grant no.2012CB722802)

References

1. X. Lu, Y. Li, W. Dai and D. Cang, Adv. Appl. Ceram. 115 (2016) 13-20.
2. C.Q. Ye, F. He, H. Shu, H. Qi, Q.P. Zhang, P.Y. Song and J.L. Xie, Mater. Des. 86 (2015) 782-787.
3. W.H. Zheng, H. Cao, J.B. Zhong, S.Y. Qian, Z.G. Peng and C.H. Shen, J. Non-Cryst. Solids 409 (2015) 27-33.
4. B.W. Li, H.X. Li, X.F. Zhang, X.L. Jia and Z.C. Sun, Int. J. Miner. Metall. Mater. 22 (2015) 1342-1349.
5. B.W. Li, L.B. Deng, X.F. Zhang, S.L. Ouyang, Y.S. Du, X.B. Liu and X.L. Jia, Int. J. Appl. Ceram. Technol. 12 (2015) 41-48.
6. B.W. Li, Y.S. Du, X.F. Zhang, X.L. Jia, M. Zhao and H. Chen, J. Ceram. Process Res. 15 (2014) 325-330.
7. B.W.Li, Y.S.Du, X.F.Zhang, M. Zhao and H.Chen, Environ. Prog. Sustainable Energy. 34 (2015) 420-426.
8. H.Chen, B.W.Li, M. Zhao, X.F.Zhang, X.L.Jia and Y.S.Du, Acta Phys. Sin. 64(2015) 196201-196208.
9. P. Pisciella and M. Pelino, J. Eur. Ceram. Soc. 25 (2005) 1855-1861.
10. A. Karamanov, G. Taglieri and M. Pelino, J. Am. Ceram. Soc. 82 (1999) 3012-3016.
11. N. Lonnroth and Y.Z. Yue, J. Non-Cryst. Solids 354 (2008) 1190-1193.
12. A. Karamanov and M. Pelino, J. Non-Cryst. Solids 281 (2001) 139-151.
13. A.A. Francis, Mater. Res. Bull. 41 (2006) 1146-1154.
14. Salwa A.M. Abdel-Hameed and Abeer M. El Kady, J. Adv. Res. 3(2012)167-175.
15. K. Sharma, Sher Singh, C.L.Prajapat, S.Bhattacharya, Jagannath, M.R.Singh, S.M. Yusuf and G.P.Kothiyal, J. Magn. Magn. Mater. 321(2009)3821-3828.
16. A. Goel, E. R. Shaaban, J.B. Oliveira, M.A. Sá, Maria J. Pascual and José M.F. Ferreira, Solid State Ionics 186 (2011) 59-68.
17. B.W. Li, Y.S. Du, X.F. Zhang, X.L. Jia, M. Zhao and H. Chen, Trans. Ind. Ceram. Soc. 72 (2013) 119-123.
18. S.M. Wang, F.H. Kuang, Q.Z. Yan, C.C. Ge and L.H. Qi, J. Alloys Compd. 509 (2011) 2819-2823.
19. S.M. Salmann, S.N. Salama and H.A. Abo-Mosallam, Ceram. Int. 41 (2015) 1521-1529.
20. K. Zhang, B. Li and W. Wu, Adv. Appl. Ceram. 114 (2015) 121-125.
21. K. Sharma, M.N. Deo and G.P. Kothiyal, J. Non-Cryst. Solids. 358 (2012) 1886-1891.
22. D.P. Mukherjee, A.R. Molla and S.K. Das, J. Non-Cryst. Solids 433 (2016) 51-59.
23. A. Karamanov, P. Pisciella and M. Pelino, J. Eur. Ceram. Soc. 20 (2000) 2233-2237.
24. O. Ozturk, T. Gokcen, S. Cavdar, H. Koralay and A.T. Tasci, J. Therm. Anal. Calorim. 123 (2016) 1073-1082.
25. P. Sellappan, T. Rouxel, F. Celarie, E. Becker, P. Houizot and R. Conradt, Acta Mater. 61 (2013) 5949-5965.
26. T. Wakihara, J. Tatami, K?Komeya, T?Meguro, A?Kidari, S?Hampshire and M.J. Pomeroy, J. Eur. Cera. Soc. 32(2012)1157-1161.
27. H. Shao, K.M. Liang, F?Zhou, G.L?Wang and A.M?Hu, Mater?Res?Bull?40(2005)499-506.
28. T. Toya, Y. Tamura, Y. Kameshima and K. Okada, Ceram. Int. 30 (2004) 983-989.